Available online at www.sciencedirect.com

ScienceDirect

Nuclear Physics B 920 (2017) 221–231

NUCLEAR PHYSICS B

www.elsevier.com/locate/nuclphysb

Inhibition of the Fermi velocity renormalization in a graphene sheet by the presence of a conducting plate

Jeferson Danilo L. Silva [a,*], Alessandra N. Braga [a], Wagner P. Pires [a,b], Van Sérgio Alves [a], Danilo T. Alves [a], E.C. Marino [c]

[a] *Faculdade de Física, Universidade Federal do Pará, 66075-110 Belém, Brazil*
[b] *Programa de Ciências Exatas, Universidade Federal do Oeste do Pará, 68040-470 Santarém, Brazil*
[c] *Instituto de Física, Universidade Federal do Rio de Janeiro, 21941-972 Rio de Janeiro, Brazil*

Received 1 December 2016; received in revised form 31 March 2017; accepted 20 April 2017
Available online 26 April 2017
Editor: Hubert Saleur

Abstract

We investigate the renormalization of the Fermi velocity in a plane graphene sheet in the presence of a parallel conducting plate. We use the pseudo-quantum electrodynamics to describe the Coulombian interaction between the electrons, but taking into account that this interaction is changed by the conducting plate. Incorporating the influence of the plate into the gauge field, we obtain the correspondent photon propagator and electron self-energy, showing that the logarithmic renormalization of the Fermi velocity is inhibited by the presence of the plate. Our result may be useful as an alternative way to control the electronic properties of graphene.

1. Introduction

There are several motivations for investigating properties of charged particles constrained to move on a plane. For instance, the quantum Hall effect [1], high-temperature superconductivity

* Corresponding author.
E-mail addresses: jeferson.silva@icen.ufpa.br (J.D.L. Silva), alessandrabg@ufpa.br (A.N. Braga), wagner.pires@ufopa.edu.br (W.P. Pires), vansergi@ufpa.br (V.S. Alves), danilo@ufpa.br (D.T. Alves), marino@if.ufrj.br (E.C. Marino).

http://dx.doi.org/10.1016/j.nuclphysb.2017.04.014

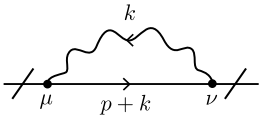

Fig. 1. One-loop electron self-energy diagram.

[2], and the graphene, a system with the thickness of a carbon atom organized in a honeycomb lattice which has two inequivalent Dirac points (K and K') associated to a valley degree of freedom [3]. Using a tight-binding approach, the electronic band structure of graphene exhibits particle–hole symmetry and, at low-energies, the dispersion relation shows a linear dependence on the momentum, namely, $E_{\pm}(\mathbf{k}) \approx \pm v_F |\mathbf{k}|$, where v_F is the bare Fermi velocity ($v_F \approx c/300$, where c is the speed of light). Therefore, electrons in graphene at low-energies can be effectively described in terms of a massless Dirac Lagrangian. In such examples of two-dimensional systems, the fundamental physical properties are determined from the behavior of the electron dynamics and, in all realistic physical applications, although the electrons are constrained to a plane, the electromagnetic field is not. In 1993 Marino [4], taking as starting point the quantum electrodynamics (QED) in $3+1$ dimensions in Euclidian space, namely

$$\mathcal{L}_{\rm QED} = \frac{1}{4} F_{\mu\nu} F^{\mu\nu} + \mathcal{L}_{\rm D} + j^{\mu} A_{\mu} - \frac{\xi}{2} A_{\mu} \partial^{\mu} \partial^{\nu} A_{\nu}, \tag{1}$$

built an effective and complete description in $2+1$ dimensions for electronic systems moving on a plane, but interacting as particles in $3+1$ dimensions. This effective theory is given by

$$\mathcal{L}_{\rm PQED} = \frac{1}{2} \frac{F_{\mu\nu} F^{\mu\nu}}{(-\Box)^{1/2}} + \mathcal{L}_{\rm D} + j^{\mu} A_{\mu} - \frac{\xi}{2} A_{\mu} \frac{\partial^{\mu} \partial^{\nu}}{(-\Box)^{1/2}} A_{\nu}, \tag{2}$$

and it is denominated pseudo-quantum electrodynamics (PQED), and sometimes it is also called reduced quantum electrodynamics [5]. In Eq. (2), $\Box$ is the d'Alembertian operator, $\mathcal{L}_{\rm D}$ stands for the Dirac's Lagrangian while the last term corresponds to the gauge fixing term. Despite the nonlocality of the Maxwell term in Eq. (2), the theory satisfies causality [6], the Huygens principle and preserves unitarity [7]. In addition it reproduces the static Coulombian potential ($\propto 1/r$), instead of the peculiar logarithmic one from QED in $2+1$ dimensions ($\propto \ln r$). Recently, PQED was used in the description of several graphene properties [8–10].

From Eq. (2), one obtains the free photon propagator in Euclidean space,

$$\Delta^{(0)}_{\mu\nu}(k) = \frac{1}{2\sqrt{k^2}} \left[\delta_{\mu\nu} - \left(1 - \frac{1}{\xi} \right) \frac{k_{\mu} k_{\nu}}{k^2} \right], \tag{3}$$

where $k_{\mu} = (k_0, \mathbf{k})$ and $\mathbf{k} = (k_1, k_2)$. In the nonretarded regime, considering the Feynman gauge ($\xi = 1$), it becomes

$$\Delta^{(0)}_{\mu\nu}(k_0 = 0, |\mathbf{k}|) = \frac{1}{2|\mathbf{k}|} \delta_{0\mu} \delta_{0\nu}, \tag{4}$$

which leads to the Coulombian interaction for static charges. In this regime, the electron self-energy in a graphene sheet (see Fig. 1) was calculated in Ref. [11] (see also Refs. [12–14]), and the result in one-loop order is

$$\Sigma_0(\mathbf{p}) = \frac{e^2 (\mathbf{p} \cdot \boldsymbol{\gamma})}{16\pi} \ln \frac{\Lambda}{|\mathbf{p}|}, \tag{5}$$

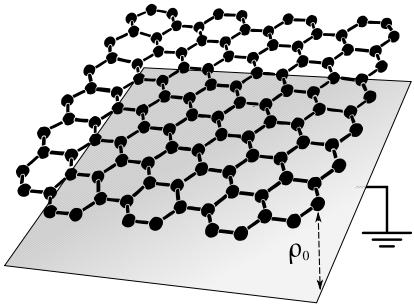

Fig. 2. Illustration of a graphene sheet parallel to a grounded conducting plate, separated by a distance ρ_0.

where e is the nonrenormalized coupling constant, $\gamma^\mu = (\gamma^0, \boldsymbol{\gamma})$ stands for the Dirac matrices, and Λ is an ultraviolet cutoff introduced in the momentum integrals. From Eq. (5), the renormalized Fermi velocity $v_F^R(|\mathbf{p}|)$ with external momentum p reads [11]

$$v_F^R(|\mathbf{p}|) = v_F\left(1 + \frac{\alpha_F}{4}\ln\frac{\Lambda}{|\mathbf{p}|}\right), \tag{6}$$

where $\alpha_F = e^2/(4\pi v_F)$ is the graphene fine structure constant. The Fig. 2c found in Ref. [15] exhibits experimental results in good agreement with the theoretical prediction shown in Eq. (6).

In graphene, as well as in other two-dimensional systems, the transport properties of the electrons can be controlled with the application of external electric and magnetic fields, or changing the geometry or topology of the sample [3,16]. The present paper is focused on investigating the effects of a grounded conducting plate on the Fermi velocity renormalization in a suspended graphene sheet (see Fig. 2). The presence of the plate imposes boundary conditions to the electromagnetic field and, when the dimensional reduction from Eq. (1) to Eq. (2) incorporates the effects of the boundary conditions imposed to the electromagnetic field in $3+1$ dimensions, the influence of such external conditions is carried into PQED. This procedure generates models that we shall denominate cavity pseudo-quantum electrodynamics (Cavity PQED), a term suggested in analogy with the Cavity QED, a branch of QED which investigates how the boundary conditions imposed by the environment influence the radiative properties of atomic systems [17–20].

The paper is organized as follows. In Sec. 2, we obtain an expression for the photon propagator modified due to the presence of a grounded perfectly conducting plate. In Sec. 3, using the results from the previous section, we calculate the electron self-energy in one-loop order, and the result is then used to obtain an expression for the renormalized Fermi velocity in a graphene sheet near a grounded conducting plate. In Sec. 4 we present a summary of the results and our final remarks.

2. The modified photon propagator

Let us start by considering an electric charge e at a distance ρ_0 from a grounded and perfectly conducting plate. In this situation, the electrostatic potential vanishes on the plate (namely, it obeys the Dirichlet boundary condition). By the image method (which arises as a consequence of the uniqueness of the Laplace equation solutions), the potential V for this configuration at an arbitrary point P also separated by a distance ρ_0 from the plate is (see Fig. 3)

$$V(P) = \frac{e}{4\pi}\left(\frac{1}{|\mathbf{r}|} - \frac{1}{|\mathbf{r}|'}\right), \tag{7}$$

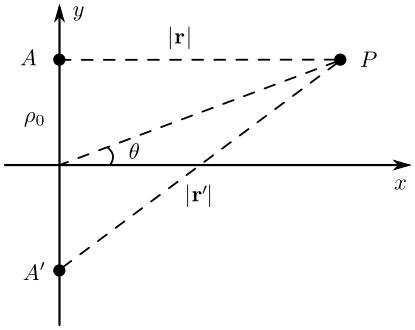

Fig. 3. The charge and its image are located, respectively, at the points A and A', the conducting plate is located at the plane $y = 0$, and P is an arbitrary point of the plane $y = \rho_0$.

where $|\mathbf{r}|$ ($|\mathbf{r}|'$) is the distance between the charge (image) and the point P, which can be rewritten as

$$|\mathbf{r}| = \rho_0 \cot\theta \qquad \text{and} \qquad |\mathbf{r}|' = \rho_0\sqrt{\cot^2\theta + 4}, \tag{8}$$

with the parameter θ being the angle shown in Fig. 3. Also, the unit system was set so that $\epsilon_0 = 1$. Therefore,

$$V(\theta) = \frac{e}{4\pi\rho_0}\left[\tan\theta - \frac{1}{\sqrt{\cot^2\theta + 4}}\right]. \tag{9}$$

Notice that the potential is azimuthally symmetric. From this static potential, we can get the "00" component of the photon propagator for electrons constrained to the plane $y = \rho_0$, via the inverse Fourier transform, which is given by (see, for instance, Ref. [21])

$$\Delta_{00}^{(0)}(k_0 = 0, |\mathbf{k}|) = \frac{1}{e^2}\int \mathrm{d}^2\mathbf{r}\, \mathrm{e}^{-i\mathbf{k}\cdot\mathbf{r}} e V(\theta), \tag{10}$$

with $\mathbf{k}$ and $\mathbf{r}$ being restricted to the plane $y = \rho_0$ (see Fig. 3), so that

$$\mathrm{d}^2\mathbf{r} = |\mathbf{r}|\,\mathrm{d}\varphi\,\mathrm{d}|\mathbf{r}| = -\rho_0^2 \cot\theta \csc^2\theta\,\mathrm{d}\theta\,\mathrm{d}\varphi, \tag{11}$$

and

$$\mathbf{k}\cdot\mathbf{r} = |\mathbf{k}||\mathbf{r}|\cos\varphi = |\mathbf{k}|\rho_0 \cot\theta\cos\varphi, \tag{12}$$

where φ is integrated from 0 to 2π and θ from $\pi/2$ to 0 [since $\theta = \pi/2$ corresponds to $|\mathbf{r}| = 0$ and $\theta \to 0$ corresponds to $|\mathbf{r}| \to \infty$ (see Fig. 3)], thus we can write

$$\Delta_{00}^{(0)}(|\mathbf{k}|) = \frac{\rho_0}{4\pi}\int \mathrm{d}\theta\,\mathrm{d}\varphi \csc^2\theta\left[\frac{\cot\theta}{\sqrt{\cot^2\theta + 4}} - 1\right]\exp\left(-i|\mathbf{k}|\rho_0\cot\theta\cos\varphi\right), \tag{13}$$

where it should be understood that $k_0 = 0$ in $\Delta_{00}^{(0)}(|\mathbf{k}|)$. By integrating in φ one gets

$$\Delta_{00}^{(0)}(|\mathbf{k}|) = \frac{\rho_0}{2}\int_0^{\pi/2} \mathrm{d}\theta \csc^2\theta\left[1 - \frac{\cot\theta}{\sqrt{\cot^2\theta + 4}}\right] J_0(|\mathbf{k}|\rho_0\cot\theta), \tag{14}$$

where J_0 is the Bessel function of first kind. The change of variables $u = |\mathbf{k}|\rho_0 \cot\theta$ makes the integration in θ straightforward since [22]

$$\int_0^\infty \mathrm{d}u \, \frac{u J_0(u)}{\sqrt{u^2+a^2}} = \mathrm{e}^{-a}. \tag{15}$$

Therefore, after integration in θ, we get

$$\Delta_{00}^{(0)}(\rho_0, |\mathbf{k}|) = \frac{1}{2|\mathbf{k}|}\left[1 - \exp(-2\rho_0|\mathbf{k}|)\right]. \tag{16}$$

The first term in the right-hand side of Eq. (16) is the propagator in absence of plate, as shown in Eq. (4), recovered when $\rho_0 \to \infty$, and the exponential term arises due to the present of the plate.

Next, we shall use Eq. (16) for the photon propagator to obtain the new expression for the electron self-energy, from which we get the renormalized Fermi velocity.

3. One-loop electron self-energy and Fermi velocity renormalization

As the massless electrons move with a Fermi velocity in a graphene sheet, instead of the speed of light, the Dirac's Lagrangian is given by

$$\mathcal{L}_\mathrm{D} = \bar{\psi}_a \left(i\gamma^0 \partial_0 + i v_F \boldsymbol{\gamma} \cdot \nabla \right) \psi_a, \tag{17}$$

where $\bar{\psi}_a = \psi_a^\dagger \gamma^0$, and a is a flavor index representing a sum over valleys K and K', γ^μ are rank-4 Dirac matrices and $\psi_a^\dagger = \left(\psi_{A\uparrow}^\star \; \psi_{A\downarrow}^\star \; \psi_{B\uparrow}^\star \; \psi_{B\downarrow}^\star\right)_a$ a four-component Dirac spinor representing electrons in sublattices A and B in graphene, with different spin orientations.

The Lagrangian above leads to the following bare fermion propagator

$$S_F^{(0)}(k^\mu) = \frac{k_0\gamma^0 + v_F \mathbf{k}\cdot\boldsymbol{\gamma}}{k_0^2 + v_F^2|\mathbf{k}|^2}. \tag{18}$$

If we consider only the static case ($v_F/c \ll 1$), which means that the vertex interaction will be $e\gamma^0$, the one-loop electron self-energy (see Fig. 1) reads (since this calculation does not involve a fermion loop, it is sufficient to consider only one species of fermions)

$$\begin{aligned}\Sigma(\rho_0, \mathbf{p}) &= e^2 \int \frac{\mathrm{d}^2\mathbf{k}}{(2\pi)^2} \frac{dk_0}{2\pi} \gamma^0 S_F^{(0)}(k^\mu + p^\mu)\gamma^0 \Delta_{00}^{(0)}(\rho_0, |\mathbf{k}|) \\ &= \frac{e^2}{2} \int \frac{\mathrm{d}^2\mathbf{k}}{(2\pi)^2} \frac{(\mathbf{k}+\mathbf{p})\cdot\boldsymbol{\gamma}}{|\mathbf{k}+\mathbf{p}|} \Delta_{00}^{(0)}(\rho_0, |\mathbf{k}|).\end{aligned} \tag{19}$$

In the last equation we used $\gamma^0 \boldsymbol{\gamma} \gamma^0 = -\boldsymbol{\gamma}$. The electron self-energy can be written as

$$\Sigma(\rho_0, \mathbf{p}) = \Sigma_0(\mathbf{p}) + \tilde{\Sigma}(\rho_0, \mathbf{p}), \tag{20}$$

where Σ_0 is the self-energy in the absence of the plate (recovered when $\rho_0 \to \infty$), and $\tilde{\Sigma}$ is the contribution due to the presence of the conducting plate, namely

$$\Sigma_0(\mathbf{p}) = \frac{e^2}{2} \int \frac{\mathrm{d}^2\mathbf{k}}{(2\pi)^2} \frac{(\mathbf{k}+\mathbf{p})\cdot\boldsymbol{\gamma}}{|\mathbf{k}+\mathbf{p}|} \frac{1}{2|\mathbf{k}|}, \tag{21}$$

$$\tilde{\Sigma}(\rho_0, \mathbf{p}) = -\frac{e^2}{2} \int \frac{\mathrm{d}^2\mathbf{k}}{(2\pi)^2} \frac{(\mathbf{k}+\mathbf{p})\cdot\boldsymbol{\gamma}}{|\mathbf{k}+\mathbf{p}|} \frac{\exp(-2\rho_0|\mathbf{k}|)}{2|\mathbf{k}|}. \tag{22}$$

The integral in Eq. (21) is ultraviolet divergent, but a cutoff $\Lambda = |\mathbf{k}|_{\max}$ can be used in order to regularize it, which results in Eq. (5) (in accordance to Refs. [11–14]). On the other hand, the term due to the plate, given by Eq. (22), is naturally finite at the ultraviolet since the exponential factor in the integrand vanishes very fast. However, since the cutoff Λ used to regularize (21) has physical meaning (it is of the order of the inverse lattice parameter of graphene), it must be also considered in the term due to the plate (22), even this being finite at the ultraviolet. As we shall see later, it plays an important role in the Fermi velocity renormalization.

To perform the integrals shown in Eqs. (21) and (22), one can use elliptical coordinates (see, for instance, Refs. [12,23]), namely

$$k_1 = \frac{|\mathbf{p}|}{2}\left(\cosh\mu\cos\nu - 1\right), \quad k_2 = \frac{|\mathbf{p}|}{2}\sinh\mu\sin\nu, \tag{23}$$

where $\nu \in [0, 2\pi)$ and $\mu \in [0, \infty)$, thus

$$|\mathbf{k}| = \frac{|\mathbf{p}|}{2}\left(\cosh\mu - \cos\nu\right). \tag{24}$$

Since $|\mathbf{k}|$ cannot assume values greater than the cutoff Λ ($|\mathbf{k}| \leq \Lambda$), the variable μ must be limited by a maximum value μ_Λ (which depends on ν). Therefore, from Eq. (24),

$$\cosh\mu_\Lambda = \frac{2\Lambda}{|\mathbf{p}|} + \cos\nu. \tag{25}$$

Using Eq. (23) into Eq. (22), and taking into account that $\mu \leq \mu_\Lambda$ [with μ_Λ being defined in Eq. (25)], the term of the electron self-energy that arises due to the plate becomes

$$\tilde{\Sigma}(\rho_0, \mathbf{p}) = -\frac{(\mathbf{p}\cdot\boldsymbol{\gamma})e^2}{16\pi}\left[L_1(\rho_0|\mathbf{p}|) + L_2(\rho_0|\mathbf{p}|)\right], \tag{26}$$

where

$$L_1(\rho_0|\mathbf{p}|) = \int_0^{2\pi} \mathrm{d}\nu \int_0^{\mu_\Lambda} \mathrm{d}\mu\ f(\rho_0|\mathbf{p}|;\mu,\nu), \tag{27}$$

$$L_2(\rho_0|\mathbf{p}|) = \int_0^{2\pi} \mathrm{d}\nu\cos\nu \int_0^{\mu_\Lambda} \mathrm{d}\mu\cosh\mu f(\rho_0|\mathbf{p}|;\mu,\nu), \tag{28}$$

and

$$f(\rho_0|\mathbf{p}|;\mu,\nu) = \frac{1}{2\pi}\exp\left[\rho_0\,|\mathbf{p}|\,(\cos\nu - \cosh\mu)\right]. \tag{29}$$

In Eqs. (27) and (28) the integration in μ must be done first since μ_Λ depends on ν.

Equations (27) and (28) are very stable for numerical integration due to the decreasing exponential factor present into $f(\rho_0|\mathbf{p}|;\mu,\nu)$. To illustrate this assertion, some qualitative plots of the integrands of Eqs. (27) and (28) are shown in Fig. 4, from which one can see that the integrands vanish very fast, indeed. In the following, we shall leave clear the role played by the cutoff Λ in these naturally finite integrals.

In situations where the distance between the graphene sheet and the conducting plate is very short as, for instance, distances of the order of the lattice parameter, the upper limit μ_Λ of the integrals in Eqs. (27) and (28) prevents spurious contributions to be computed in the electron self-energy, what would occur if the integrals were up to infinity (see the thick lines in Fig. 4a,

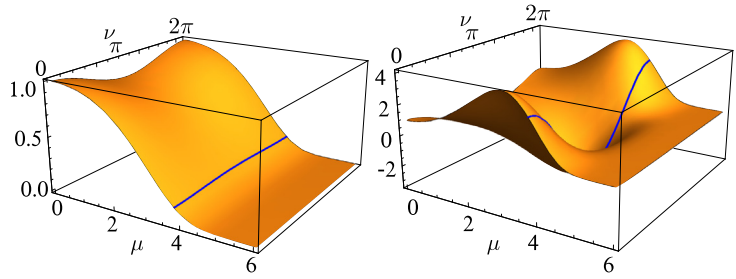

(a) Integrands of L_1 (left) and L_2 (right) with $\rho_0 = 1/\Lambda$.

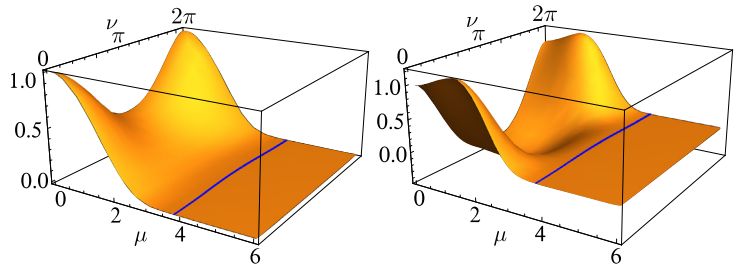

(b) Integrands of L_1 (left) and L_2 (right) with $\rho_0 = 5/\Lambda$.

Fig. 4. Integrands of L_1 and L_2 [Eqs. (27) and (28)] as functions of μ and ν, with $|\mathbf{p}| = \Lambda/10$. Fig. 4a shows the integrands of L_1 (left) and L_2 (right) with $\rho_0 = 1/\Lambda$. Fig. 4b shows the integrands of L_1 (left) and L_2 (right) with $\rho_0 = 5/\Lambda$. The thick lines are indicating μ_Λ, which delimits the region of integration.

which represent the cutoff μ_Λ, and notice that the integrands have not vanished yet at these lines). However, a small increase in the distance between the graphene sheet and the plate is enough to make the integrands of Eqs. (27) and (28) vanish before reaching the cutoff μ_Λ (see the thick lines in Fig. 4b and notice that, in this case, the integrands have already vanished at these lines). Therefore, one may consider, in good approximation, the upper limit of integration as infinity in this case, allowing the integrals to be computed exactly, resulting in [22]

$$L_1(\rho_0|\mathbf{p}|) \approx I_0(\rho_0|\mathbf{p}|)K_0(\rho_0|\mathbf{p}|), \tag{30}$$

$$L_2(\rho_0|\mathbf{p}|) \approx I_1(\rho_0|\mathbf{p}|)K_1(\rho_0|\mathbf{p}|), \tag{31}$$

where I_ν and K_ν are the modified Bessel functions of first and second kind, respectively.

The electron self-energy in the presence of the plate is given by

$$\Sigma(\rho_0, \mathbf{p}) = \frac{e^2(\mathbf{p}\cdot\boldsymbol{\gamma})}{16\pi}\left[\ln\frac{\Lambda}{|\mathbf{p}|} - L_1(\rho_0|\mathbf{p}|) - L_2(\rho_0|\mathbf{p}|)\right], \tag{32}$$

where L_1 and L_2 are given by Eqs. (27) and (28) [or approximately by Eqs. (30) and (31)].

The complete fermion propagator can be written in terms of the electron self-energy as

$$S_F(k^\mu) = \frac{1}{-k_\mu\gamma^\mu + \Sigma(k^\mu)}, \tag{33}$$

from which we obtain the following renormalized Fermi velocity in the presence of a grounded conducting plate,

$$\frac{v_F^R(\rho_0, |\mathbf{p}|)}{v_F} = 1 + \frac{\alpha_F}{4}\left[\ln\frac{\Lambda}{|\mathbf{p}|} - L_1(\rho_0|\mathbf{p}|) - L_2(\rho_0|\mathbf{p}|)\right]. \tag{34}$$

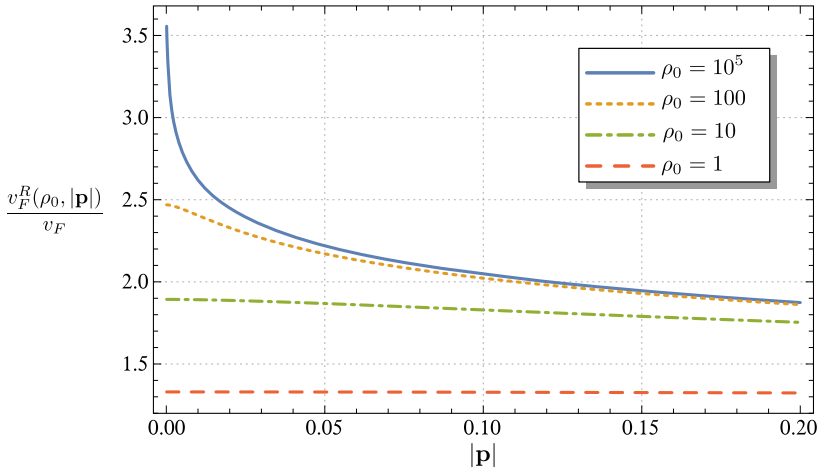

Fig. 5. Renormalized Fermi velocity as function of the external momentum $|\mathbf{p}|$, for several values of ρ_0 (considering $\Lambda = \alpha_F = 1$).

Since $L_1(\rho_0|\mathbf{p}|)$ and $L_2(\rho_0|\mathbf{p}|)$ can be written in terms of Bessel functions, as shown in Eqs. (30) and (31), in the limit of $\rho_0|\mathbf{p}| \ll 1$ one gets [22]

$$I_0(\rho_0|\mathbf{p}|) = 1 + \mathcal{O}\left(\rho_0^2|\mathbf{p}|^2\right), \tag{35}$$

$$I_1(\rho_0|\mathbf{p}|) = \frac{\rho_0|\mathbf{p}|}{2} + \mathcal{O}\left(\rho_0^3|\mathbf{p}|^3\right), \tag{36}$$

$$K_0(\rho_0|\mathbf{p}|) = \ln\frac{2}{\rho_0|\mathbf{p}|} + \mathcal{C} + \mathcal{O}\left(\rho_0^2|\mathbf{p}|^2\right), \tag{37}$$

$$K_1(\rho_0|\mathbf{p}|) = \frac{1}{\rho_0|\mathbf{p}|} - \frac{\rho_0|\mathbf{p}|}{2}\left(\ln\frac{2}{\rho_0|\mathbf{p}|} + \mathcal{C} + \frac{1}{2}\right) + \mathcal{O}\left(\rho_0^3|\mathbf{p}|^3\right), \tag{38}$$

where $\mathcal{C} \approx 0.577215$ is the Euler–Mascheroni constant. In this limit, Eq. (34) becomes

$$\frac{v_F^R(\rho_0,|\mathbf{p}|)}{v_F} = 1 + \frac{\alpha_F}{4}\left[\ln\frac{\Lambda\rho_0}{2} - \mathcal{C} - \frac{1}{2} + \frac{\rho_0^2|\mathbf{p}|^2}{4}\ln\frac{1}{\rho_0|\mathbf{p}|} + \mathcal{O}\left(\rho_0^2|\mathbf{p}|^2\right)\right]. \tag{39}$$

Therefore, in the limit $\rho_0|\mathbf{p}| \ll 1$, $L_1(\rho_0|\mathbf{p}|)$ has a logarithmic behavior that compensates the divergent term $\ln(\Lambda/|\mathbf{p}|)$ in Eq. (34). This is responsible for the behavior of the renormalized Fermi velocity shown in Fig. 5 and discussed in the following.

Notice that the negative signs of L_1 and L_2 in the right hand side of Eq. (34), along with the observation that $L_1(\rho_0|\mathbf{p}|) > 0$ and $L_2(\rho_0|\mathbf{p}|) > 0$, lead to the conclusion that the Fermi velocity renormalization is inhibited by the presence of the conducting plate. The behavior of the renormalized Fermi velocity given by Eq. (34) can be visualized in Fig. 5, and the ratio between the Fermi velocity given by Eq. (34) and the renormalized Fermi velocity in the absence of the plate is shown in Fig. 6. In these figures, the solid lines, obtained by making $\rho_0 = 10^5/\Lambda$ (the distance between the graphene sheet and the plate is 10^5 times the lattice parameter), can be considered a good approximation to the result without the plate found in the literature [Eq. (6)], which, in turn, is associated to the solid line in Fig. 2c found in Ref. [15]. We can see that for $\rho_0 = 100/\Lambda$ (the dotted lines, of Figs. 5 and 6), a considerable inhibition of $v_F^R(\rho_0, |\mathbf{p}|)$ occurs for

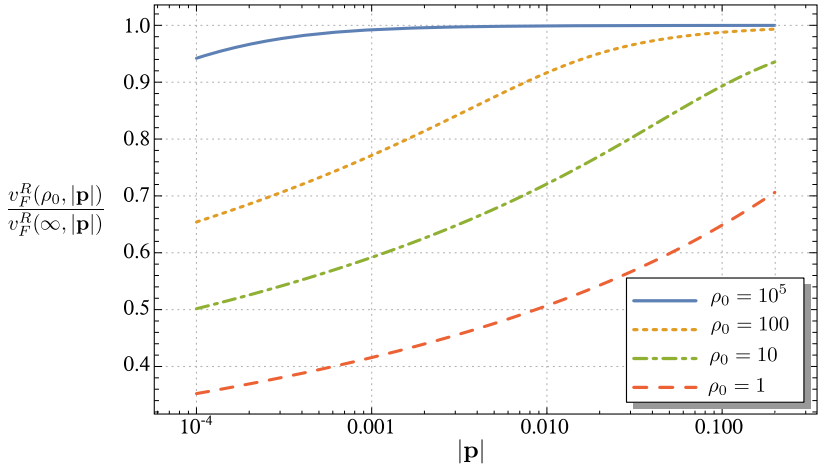

Fig. 6. Ratio between the renormalized Fermi velocity with and without the plate as function of the external momentum $|\mathbf{p}|$, for several values of ρ_0 (considering $\Lambda = \alpha_F = 1$).

$|\mathbf{p}| \to 0$. For $\rho_0 = 10/\Lambda$ and $\rho_0 = 1/\Lambda$, the inhibition of $v_F^R(\rho_0, |\mathbf{p}|)$ becomes more expressive, with the characteristic that $v_F^R(\rho_0, |\mathbf{p}|)/v_F \approx$ constant.

4. Final remarks

We considered the electron–electron Coulombian interaction in graphene described via PQED [Eq. (2)]. Moreover, we introduced the Cavity PQED — a branch of PQED that includes effects of boundary conditions imposed by the environment to the electromagnetic field. We investigated the renormalization of the Fermi velocity in a graphene sheet in the presence of a perfectly conducting and grounded plate. Our results showed that the well-known logarithmic renormalization of the Fermi velocity [see Eq. (6)] is inhibited, as shown in Eqs. (34) and (39), and Figs. 5 and 6. This inhibition occurs because the effective interaction of the electrons in a graphene sheet is affected by the presence of the plate, changing the photon propagator (16) and, consequently, the electron self-energy (20).

For small distances between the graphene sheet and the plate, for instance $\rho_0 \approx 1/\Lambda$ or $\rho_0 \approx 10/\Lambda$ (respectively, dashed and dot-dashed lines in Figs. 5 and 6), our model shows a significant inhibition of the renormalized Fermi velocity. However, even for larger distances in comparison to the graphene lattice parameter, for instance $\rho_0 \approx 100/\Lambda$ or $\rho_0 \approx 10^5/\Lambda$, (respectively, dotted and solid lines in Figs. 5 and 6) the renormalized Fermi velocity will be still inhibited. The inhibition becomes more significant for lower values of the external momentum. In the limit $\rho_0 \to \infty$ (the distance between the graphene sheet and the plate goes to infinity), our results are in agreement with those found in the literature [11–14].

Although the specific model of Cavity PQED investigated here deals with some ideal situations, our results reveal that the renormalization of the Fermi velocity can be inhibited by the presence of a conducting plate, which may be useful as an additional way to control the electronic properties of graphene, as usually done via external electric and magnetic fields or changing the geometry or topology of the sample [3,16]. More complex models of Cavity PQED, including more realistic conditions imposed by the environment on the graphene properties, are under investigation.

Acknowledgements

We thank C. M. Smith, J. F. de Medeiros Neto, L. O. Nascimento, F. S. S. Rosa, C. Farina, M. E. Rodrigues, and V. Dmitriev for fruitful discussions. This work was partially supported by Brazilian agencies Coordenação de Aperfeiçoamento de Pessoal de Nível Superior (CAPES), Conselho Nacional de Desenvolvimento Científico e Tecnológico (CNPq), and Fundação de Amparo à Pesquisa do Estado do Rio de Janeiro (FAPERJ).

References

[1] R.E. Prange, S.M. Girvin (Eds.), The Quantum Hall effect, Springer, New York, 1990.

[2] J.G. Bednorz, K.A. Müller, Possible high T_c superconductivity in the Ba — La — Cu — O system, in: Perspectives in Condensed Matter Physics, vol. 7, Springer, Netherlands, Dordrecht, 1993, p. 267.

[3] A.H. Castro Neto, F. Guinea, N.M.R. Peres, K.S. Novoselov, A.K. Geim, The electronic properties of graphene, Rev. Mod. Phys. 81 (2009) 109, http://dx.doi.org/10.1103/RevModPhys.81.109, arXiv:0709.1163, http://link.aps.org/doi/10.1103/RevModPhys.81.109.

[4] E.C. Marino, Quantum electrodynamics of particles on a plane and the Chern–Simons theory, Nucl. Phys. B 408 (1993) 551, http://dx.doi.org/10.1016/0550-3213(93)90379-4, arXiv:hep-th/9301034, http://www.sciencedirect.com/science/article/pii/0550321393903794.

[5] E.V. Gorbar, V.P. Gusynin, V.A. Miransky, Dynamical chiral symmetry breaking on a brane in reduced QED, Phys. Rev. D 64 (2001) 105028, http://dx.doi.org/10.1103/PhysRevD.64.105028, arXiv:hep-ph/0105059, http://link.aps.org/doi/10.1103/PhysRevD.64.105028.

[6] R.L.P.G. do Amaral, E.C. Marino, Canonical quantization of theories containing fractional powers of the d'Alembertian operator, J. Phys. A 25 (1992) 5183, http://dx.doi.org/10.1088/0305-4470/25/19/026, http://stacks.iop.org/0305-4470/25/i=19/a=026.

[7] E.C. Marino, L.O. Nascimento, V.S. Alves, C. Morais Smith, Unitarity of theories containing fractional powers of the d'Alembertian operator, Phys. Rev. D 90 (2014) 105003, http://dx.doi.org/10.1103/PhysRevD.90.105003, arXiv:1408.1637, http://link.aps.org/doi/10.1103/PhysRevD.90.105003.

[8] V.S. Alves, W.S. Elias, L.O. Nascimento, V. Juričić, F. Peña, Chiral symmetry breaking in the pseudo-quantum electrodynamics, Phys. Rev. D 87 (2013) 125002, http://dx.doi.org/10.1103/PhysRevD.87.125002, http://link.aps.org/doi/10.1103/PhysRevD.87.125002.

[9] L.O. Nascimento, V.S. Alves, F. Peña, C.M. Smith, E.C. Marino, Chiral-symmetry breaking in pseudoquantum electrodynamics at finite temperature, Phys. Rev. D 92 (2015) 025018, http://dx.doi.org/10.1103/PhysRevD.92.025018, arXiv:1503.08347, http://link.aps.org/doi/10.1103/PhysRevD.92.025018.

[10] E.C. Marino, L.O. Nascimento, V.S. Alves, C.M. Smith, Interaction induced quantum valley Hall effect in graphene, Phys. Rev. X 5 (2015) 011040, http://dx.doi.org/10.1103/PhysRevX.5.011040, http://link.aps.org/doi/10.1103/PhysRevX.5.011040.

[11] J. González, F. Guinea, M.A.H. Vozmediano, Non-Fermi liquid behavior of electrons in the half-filled honeycomb lattice (a renormalization group approach), Nucl. Phys. B 424 (1994) 595, http://dx.doi.org/10.1016/0550-3213(94)90410-3, arXiv:hep-th/9311105, http://www.sciencedirect.com/science/article/pii/0550321394904103.

[12] E. Barnes, E.H. Hwang, R.E. Throckmorton, S. Das Sarma, Effective field theory, three-loop perturbative expansion, and their experimental implications in graphene many-body effects, Phys. Rev. B 89 (2014) 235431, http://dx.doi.org/10.1103/PhysRevB.89.235431, arXiv:1401.7011, http://link.aps.org/doi/10.1103/PhysRevB.89.235431.

[13] M.A.H. Vozmediano, Renormalization group aspects of graphene, Philos. Trans. R. Soc. Lond. Ser. A 369 (2011) 2625, http://dx.doi.org/10.1098/rsta.2010.0383, arXiv:1010.5057, http://rsta.royalsocietypublishing.org/content/369/1946/2625.

[14] M.A.H. Vozmediano, F. Guinea, Effect of Coulomb interactions on the physical observables of graphene, Phys. Scr. 2012 (2012) 014015, http://dx.doi.org/10.1088/0031-8949/2012/T146/014015, arXiv:1108.0580, http://stacks.iop.org/1402-4896/2012/i=T146/a=014015.

[15] D.C. Elias, R.V. Gorbachev, A.S. Mayorov, S.V. Morozov, A.A. Zhukov, P. Blake, L.A. Ponomarenko, I.V. Grigorieva, K.S. Novoselov, F. Guinea, A.K. Geim, Dirac cones reshaped by interaction effects in suspended graphene, Nat. Phys. 7 (2011) 701, http://dx.doi.org/10.1038/nphys2049, arXiv:1104.1396, http://www.nature.com/nphys/journal/v7/n9/abs/nphys2049.html.

[16] F. de Juan, M. Sturla, M.A.H. Vozmediano, Space dependent Fermi velocity in strained graphene, Phys. Rev. Lett. 108 (2012) 227205, http://dx.doi.org/10.1103/PhysRevLett.108.227205, arXiv:1201.2656, http://link.aps.org/doi/10.1103/PhysRevLett.108.227205.
[17] E. Purcell, Spontaneous emission probabilities at radio frequencies, Phys. Rev. 69 (1946) 681, http://dx.doi.org/10.1103/PhysRev.69.674.2, http://link.aps.org/doi/10.1103/PhysRev.69.674.2.
[18] P.W. Milonni, The Quantum Vacuum: an Introduction to Electrodynamics, Academic Press, 1994.
[19] S. Haroche, Cavity quantum electrodynamics, in: J. Dalibard, J.M. Raimond, J.Z. Justin (Eds.), Fundamental Systems in Quantum Optics, vol. LIII of Proceedings of the Les Houches Summer School of Theoretical Physics, North Holland, Amsterdam, 1992.
[20] P.R. Berman, D.R. Bates, B. Bederson, Cavity Quantum Electrodynamics, Academic Press, 1994.
[21] C.D. Roberts, A.G. Williams, Dyson–Schwinger equations and their application to hadronic physics, Prog. Part. Nucl. Phys. 33 (1994) 477, http://dx.doi.org/10.1016/0146-6410(94)90049-3, arXiv:hep-ph/9403224, http://www.sciencedirect.com/science/article/pii/0146641094900493.
[22] I.S. Gradshteyn, I.M. Ryzhik, Table of Integrals, Series, and Products, Academic Press, 2007.
[23] I. Sodemann, M.M. Fogler, Interaction corrections to the polarization function of graphene, Phys. Rev. B 86 (2012) 115408, http://dx.doi.org/10.1103/PhysRevB.86.115408, arXiv:1206.3519, http://link.aps.org/doi/10.1103/PhysRevB.86.115408.